Supplementary information

Surface Contacts Strongly Influence the Elasticity and Thermal Conductivity of Silica Nanoparticle Fibers

*Yu Cang[a,b], Bohai Liu[c], Sudatta Das[b], Xiangfan Xu[c], Jingli Xie[d], Xu Deng[d], George Fytas[b]**

[a]School of Aerospace Engineering and Applied Mechanics, Tongji University, 100 Zhangwu Road, 200092, Shanghai, China.
[b]Max Planck Institute for Polymer Research, Ackermannweg 10, 55128, Mainz, Germany.
[c]Center for Phononics and Thermal Energy Science, School of Physical Science and Engineering, Tongji University, Shanghai, 200092, China.
[d]Institute of Fundamental and Frontier Sciences, University of Electronic Science and Technology of China, Chengdu, 610054, China.

Contents

1. Methods

1.1 Density characterization of silica fiber

The density $\rho = \frac{m}{V}$ of fibers is obtained from its mass m and the total volume V, where the mass m is measured by the precision balance scale and the volume V of a rectangle-shape is estimated by its three dimensions (length × width × thickness) determined from its optical images.

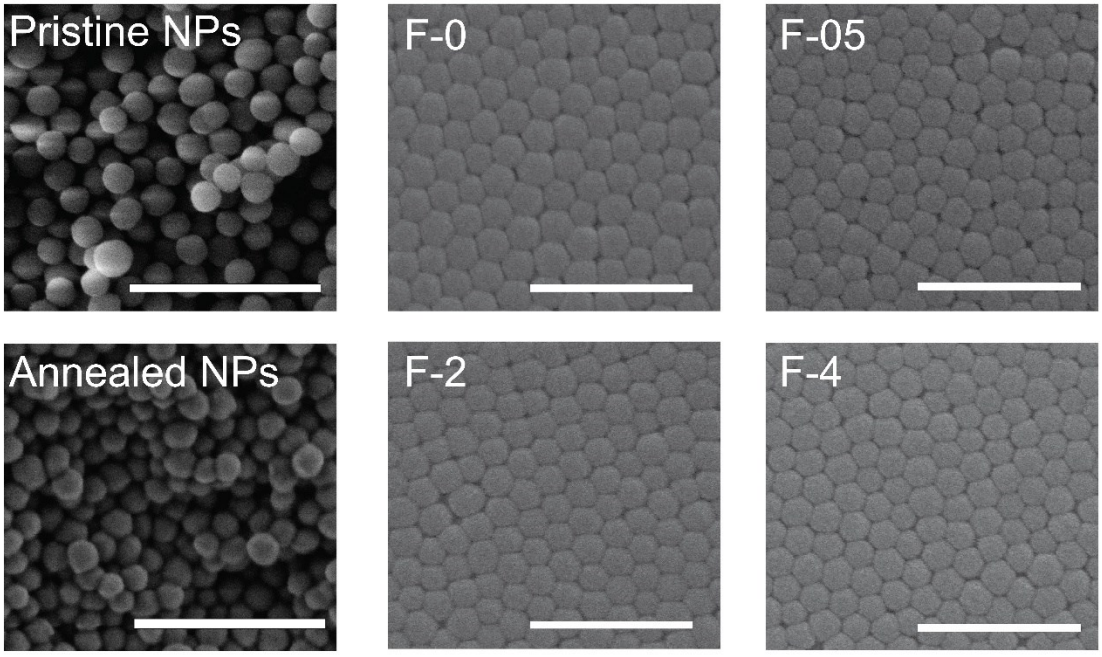

Figure S1. Scanning electron microscope (SEM) images of pristine and annealed silica nanoparticles, F-0, F-05, F-2, and F-4 as indicated. The scale bars are 500nm.

1.2 Brillouin light spectroscopy (BLS)

BLS is based on the inelastic scattering of incident light with monochromatic wavelength λ=532nm and f_i by thermally activated phonons with frequency $f=\pm(f_i-f_s)$ and wavevector $\mathbf{q}=\pm(\mathbf{k_s}-\mathbf{k_i})$; f_s and $\mathbf{k_s}$ denote the frequency and wavevector of scattered light which is

analyzed by a high resolution six pass tandem Fabry Perot interferometer. We utilized three scattering geometries to select **q** directed parallel, normal, and oblique to the film normal. (Figure S2). The resolved acoustic effective medium phonons have $f=cq/2\pi$ with c being the longitudinal (LA) or transverse (TA) sound velocity in the materials. The LA and TA phonon are selected by polarized (VV) and depolarized (VH) light combination, respectively, where the later V(H) denotes the vertically (horizontally) polarized scattered light relative to the ($\mathbf{k}_i$,$\mathbf{k}_s$) plane while the former V for the vertically polarized incident light. The magnitude of $q=(4\pi/\lambda)\sin(\alpha)$ is independent of refractive index n in the transmission geometry. While $q=\frac{4\pi\sqrt{n^2-\sin^2\alpha}}{\lambda}$ depends on n in the reflection and backscattering geometries. Due to the weak multiple scattering of particles in the air, the localized vibration of the constituent SiO_2 NPs is concurrently resolved with the independence of q.

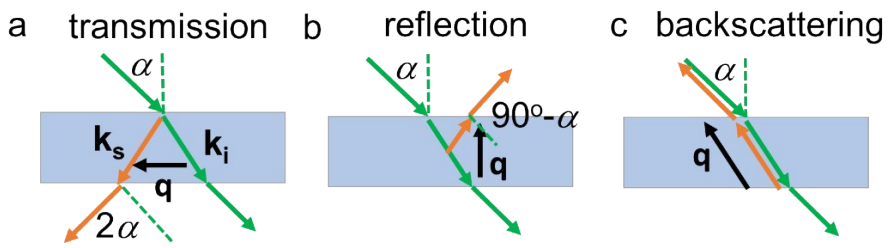

Figure S2. Scattering geometries: (a) transmission; (b) reflection; (c) backscattering. The incident light with wave vector $\mathbf{k}_i$ (green arrows) is scatted by the acoustic phonons with wave vector $\mathbf{q}=\mathbf{k}_i-\mathbf{k}_s$ (black arrow), where the scattered light with wave vector $\mathbf{k}_s$ is denoted by orange arrows. The wave vector **q** is directed parallel, normal, and oblique to the film normal at the incident and scattered angles indicated in the figures.

1.3 T-bridge method

We utilized the T-bridge method to measure the thermal conductivity κ of the silica fibers. The T-bridge approach is based on the work of M. Fujii *et al*[1] as schematically illustrated in Figure S3. Two large pads of heat sinks are connected by a narrow metal heater line, and the middle point of the heater line and a third heat sink are bridged by the tested sample. The heater line and sample are suspended in order to avoid lateral heat losses from conduction.

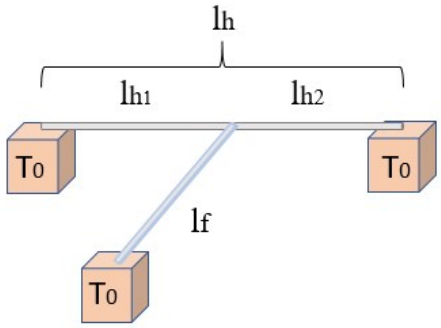

Figure S3. Schematic of a T-bridge sensor. The white rod denotes the heater line of an Al wire with a length of l_h and radius of r_h. The blue one connected to the heater line at the position of l_{h1} (l_{h1}+l_{h2}=l_h) denotes the sample to be tested with a length of l_f. The orange cubic shapes denote the heat sinks made of copper.

In this work, the heater line was fabricated by an Al wire with radius r_h of 12.5μm, and three metallic heat sinks are made of bulk copper. First, we measured the thermal conductivity of the single heater line (Al wire) without a suspended sample. Its temperature coefficient of resistance (TCR) $\beta=(dR/dT)/R_0$ was calibrated by the four-point resistance thermometry, where R and R_0 are resistance at a certain T and 300K respectively. Measurements are performed in a high-vacuum cryostat chamber (better

than 5×10^{-5}Pa) from 100 K to 300 K. Figure S4 shows the resistance of Al wire as a function of temperature, yielding β=0.00429±0.00001K^{-1}, the same as bulk Al indicating a negligible influence of contacts between the Al wire and heat sinks.

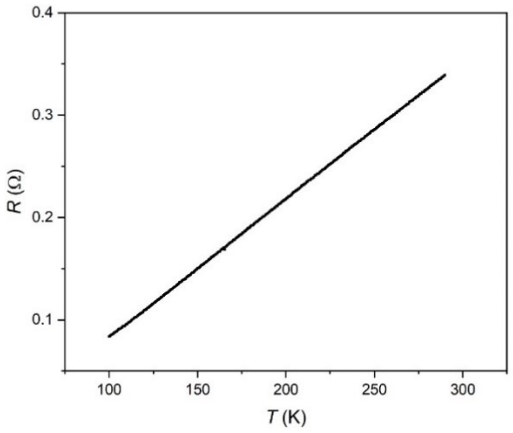

Figure S4. Resistance, *R*, of the heater line (Al wire) as a function of temperature, *T*.

Next the Al wire was heated by a DC current, *I,* generated by a current source (Keithley 6221), and the corresponding resistance, *R*, is probed by an AC current from the same source. The voltage signal of Al wire was recorded by a lock-in amplifier (SR 830). The corresponding ΔT_v (Q) is shown in Figure S5, where $\Delta T_v=(R-R_0)/\beta R_0$ is volumetric temperature rise relative to 300K and estimated based on Figure S4, and $Q=I^2R$ is heating power. The κ of the Al wire is given by

$$\kappa_h = \frac{{l_h}^2 q_v}{12\Delta T_v}$$

where $q_v=Q/V=I^2R/\pi r_h^2 l_h$ is the volumetric heat generation rate.

When a silica fiber (length: l_f; width: w_f; thickness: t_f) was suspended on the Al wire shown in Figure S3, it provides an additional path for heat transport on the Al wire. This effect is

manifested through a slightly lower ΔT_v of the Al wire relative to a bare Al wire at a given Q as shown in Figure S5.

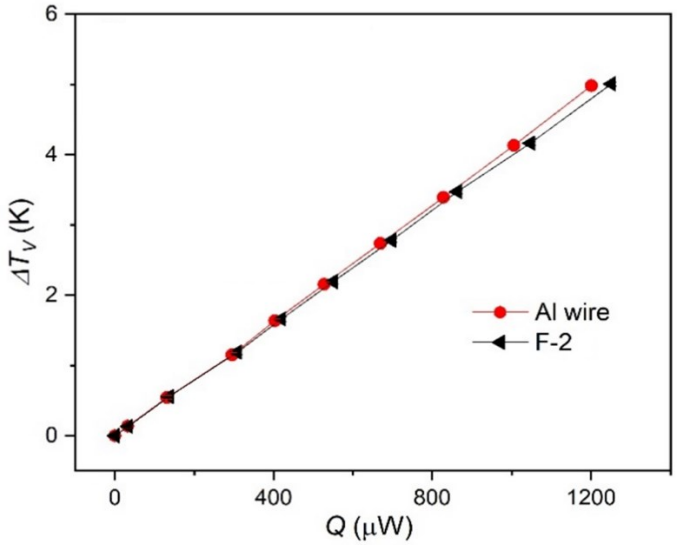

Figure S5. Temperature rise ΔT_v as a function of heating power Q in the Al wire with and without a silica fiber F-2.

The heat bypassed through the silica fiber can be treated as one-dimensional conduction and the corresponding κ of silica fiber is given by

$$\kappa_f = \frac{l_f l_h \kappa_h A_h \left(q_v l_h^3 - 12 l_h \kappa_h \Delta T_v\right)}{l_{h1} l_{h2} A_f \left\{12 l_h \kappa_h \Delta T_v - q_v \left(l_{h1}^3 + l_{h2}^3\right)\right\}}$$

where l_{h1} and l_{h2} ($=l_h$-l_{h1}) are lengths of Al wire between two heat sinks and the junction point with silica fiber; $A_h = \pi r_h^2$ and $A_f = t_f w_f$ are the areas of cross-section of heater Al wire and silica fiber, respectively; and $q_v = Q/V = I^2R/A_f l_h$. The dimensions (l_h, r_h, l_{h1}, l_{h2}, l_f, t_f, w_f) of Al wire and silica fibers were determined from its optical and/or SEM images. The validation of this method is confirmed by an additional experiment on a standard sample, Al wire with a radius of 12.5μm, as shown in Figure S6. The obtained κ=216 Wm^{-}

$^{1}K^{-1}$ for Al is slightly (~9%) lower than its typical value, which may result from contact resistance that is neglected in the calculations. Nevertheless, this method is applicable to the current samples.

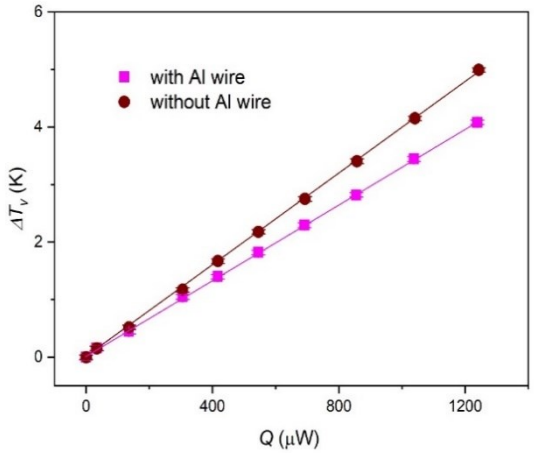

Figure S6. Temperature rise ΔT_v as a function of Q in heater line with and without a standard sample (Al wire).

The uncertainties of κ could be introduced via measurements of dimensions and electrical resistance, and temperature drifting in the vacuum chamber, which is given by

$$\frac{\delta\kappa_f}{\kappa_f} = \sqrt{\left(\frac{\delta w_f}{w_f}\right)^2 + \left(\frac{\delta t_f}{t_f}\right)^2 + \left(\frac{\delta l_h}{l_h}\right)^2 + \left(\frac{\delta l_{h1}}{l_{h1}}\right)^2 + \left(\frac{\delta l_{h2}}{l_{h2}}\right)^2 + \left(\frac{\delta l_f}{l_f}\right)^2 + \left(\frac{\delta R}{R}\right)^2 + \left(\frac{\delta T_v}{T_v}\right)^2}$$

The estimated error of dimensions (l_h, l_{h1}, l_{h2}, l_f, t_f, w_f) is ±6%; the maximum uncertainty of electrical resistance R is within 1%; the error of T_v as a results of temperature drifting was 30mK, which is calibrated by the variance of R_0 of Al wire at I=0 mA.

2. Theoretical Models.

2.1 The representative elementary volume based continuum mechanics models

Mori–Tanaka's scheme[2]: This model assumes the pores are isolated but interacted defined by a certain boundary condition. The complex calculation gives porosity p-dependent effective medium elasticities as:

$$\frac{K}{K_{NP}} = \frac{1-p}{(1-p)+\frac{p}{1-\alpha}}$$

$$\frac{G}{G_{NP}} = \frac{1-p}{(1-p)+\frac{p}{1-\beta}}$$

Where α=(1+4G_{NP}/3K_{NP})$^{-1}$ and β=(6+12G_{NP}/3K_{NP})/(15+20G_{NP}/3K_{NP}) depend on the bulk (K_{NP}) and shear (G_{NP}) moduli of nanoparticles.

Self-consistence model[3]: The model is built on the Mori-Tanaka's scheme and solves the case of pores being interconnected and percolated. The effective medium moduli of porous materials are represented as:

$$\frac{K}{K_{NP}} = \frac{1-p}{1+\left(\frac{K_{NP}}{K}-1\right)\alpha}$$

$$\frac{G}{G_{NP}} = \frac{1-p}{1+\left(\frac{G_{NP}}{G}-1\right)\beta}$$

Where α and β are same as Mori-Tanaka's scheme.

2.2 Heat transport models in porous materials

Coherent potential (CP): The CP approximation derived by Landauer was used to describe the electrical conductivity of composite materials with spherical inclusions[4]. It was

employed to predict the κ of porous Vycor glass by Cahill et al.[5] This model relates the κ to the spherical pore by

$$\kappa = \kappa_{NP}(1 - 1.5p)$$

Porosity weighted dilute medium (PWDM) model[6]: Beside the CP model, other models, such as the DF (Dilute Fluid) and the DP (Dilute Particle), were developed to take int account the size and shape of pores. Later, Hu et al[6] proposed a more general PWDM model with an empirical fitting parameter x to combine the DF and DP models, giving:

$$\kappa = \kappa_{NP}\frac{2(1-p)\kappa_{NP} + (1-2p)\kappa_{air}}{2+p)\kappa_{NP} + (1-p)\kappa_{air}}(1-p^x) + \kappa_{air}\frac{(3-2p)\kappa_{NP} + 2p\kappa_{air}}{p\kappa_{NP} + (3-p)\kappa_{air}}p^x$$

where κ_{air} is the thermal conductivity of air and the fitting parameter x(=0.1) is used in this work.

References

[1]. Fujii, M.; Zhang, X.; Xie, H.; Ago, H.; Takahashi, K.; Ikuta, T.; Abe, H.; Shimizu, T., *Physical review letters* **2005,** *95* (6), 065502.

[2]. Mori, T.; Tanaka, K., *Acta metallurgica* **1973,** *21* (5), 571-574.

[3]. Hill, R., *Journal of the Mechanics and Physics of Solids* **1965,** *13* (4), 213-222.

[4]. Landauer, R., *Journal of Applied Physics* **1952,** *23* (7), 779-784.

[5]. Cahill, D., *Microscale energy transport*, Taylor & Francis, Washington, DC, **1998**, 95-117.

[6]. Hu, C.; Morgen, M.; Ho, P. S.; Jain, A.; Gill, W. N.; Plawsky, J. L.; Wayner Jr, P. C., *Applied Physics Letters* **2000,** *77* (1), 145-147.